Single-shot volumetric laser induced fluorescence (VLIF) measurements in turbulent flows seeded with iodine

Yue Wu,[1] Wenjiang Xu,[1] Qingchun Lei,[2] and Lin Ma[1,2,*]

[1]*Department of Aerospace and Ocean Engineering, Virginia Tech, Blacksburg, VA 24061, USA*
[2]*Department of Mechanical Engineering, Virginia Tech, Blacksburg, VA 24061, USA*
[*]*linma@vt.edu*

Abstract: This work reports the experimental demonstration of single-shot visualization of turbulent flows in all three spatial dimensions (3D) based on volumetric laser induced fluorescence (VLIF). The measurements were performed based on the LIF signal of iodine (I_2) vapor seeded in the flow. In contrast to established planar LIF (PLIF) technique, the VLIF technique excited the seeded I_2 vapor volumetrically by a thick laser slab. The volumetric LIF signals emitted were then simultaneously collected by a total of five cameras from five different orientations, based on which a 3D tomographic reconstruction was performed to obtain the 3D distribution of the I_2 vapor in the target flow. Single-shot measurements (with a measurement duration of a few ns) were demonstrated in a 50 mm × 50 mm × 50 mm volume with a nominal spatial resolution of 0.42 mm and an actual resolution of ~0.71 mm in all three dimensions (corresponding to a total of 120 × 120 × 120 voxels).

OCIS codes: (300.2530) Fluorescence, laser-induced; (110.6960) Tomography.

References and links

1. R. K. Hanson, J. M. Seitzman, and P. H. Paul, "Planar laser-fluorescence imaging of combustion gases," Appl. Phys. B **50**(6), 441–454 (1990).
2. A. Lozano, B. Yip, and R. K. Hanson, "Acetone: a tracer for concentration measurements in gaseous flows by planar laser-induced fluorescence," Exp. Fluids **13**(6), 369–376 (1992).
3. I. van Cruyningen, A. Lozano, and R. K. Hanson, "Quantitative imaging of concentration by planar laser-induced fluorescence," Exp. Fluids **10**(1), 41–49 (1990).
4. T. Medford, P. Danehy, S. Jones, N. Jiang, M. Webster, W. Lempert, J. Miller, and T. Meyer, "Stereoscopic planar laser-induced fluorescence imaging at 500 kHz," in *49th AIAA Aerospace Sciences Meeting including the New Horizons Forum and Aerospace Exposition* (2011), pp. 1–14.
5. J. M. Seitzman, G. Kychakoff, and R. K. Hanson, "Instantaneous temperature field measurements using planar laser-induced fluorescence," Opt. Lett. **10**(9), 439–441 (1985).
6. Y. Zhao, C. Tong, and L. Ma, "Demonstration of a new laser diagnostic based on photodissociation spectroscopy for imaging mixture fraction in a non-premixed jet flame," Appl. Spectrosc. **64**(4), 377–383 (2010).
7. Y. Zhao, C. Tong, and L. Ma, "Assessment of a novel flow visualization technique using photodissociation spectroscopy," Appl. Spectrosc. **63**(2), 199–206 (2009).
8. Y. Zhao, C. Tong, and L. Ma, "Kinetics of I_2 and HI photodissociation with implications in flame diagnostics," Appl. Phys. B **104**(3), 689–698 (2011).
9. M. J. Dyer and D. R. Crosley, "Two-dimensional imaging of OH laser-induced fluorescence in a flame," Opt. Lett. **7**(8), 382–384 (1982).
10. C. D. Carter, J. M. Donbar, and J. F. Driscoll, "Simultaneous CH planar laser-induced fluorescence and particle imaging velocimetry in turbulent nonpremixed flames," Appl. Phys. B **66**(1), 129–132 (1998).
11. S. D. Hammack, T. Lee, K. Y. Hsu, and C. D. Carter, "High-repetition-rate OH planar laser-induced fluorescence of a cavity flameholder," J. Prop. Pow. **29**(5), 1248–1251 (2013).
12. G. Kychakoff, P. H. Paul, I. van Cruyningen, and R. K. Hanson, "Movies and 3-D images of flowfields using planar laser-induced fluorescence," Appl. Opt. **26**(13), 2498–2500 (1987).
13. J. Nygren, J. Hult, M. Richter, M. Aldén, M. Christensen, A. Hultqvist, and B. Johansson, "Three-dimensional laser induced fluorescence of fuel distributions in an HCCI engine," Proc. Combust. Inst. **29**(1), 679–685 (2002).

14. K. Y. Cho, A. Satija, T. L. Pourpoint, S. F. Son, and R. P. Lucht, "High-repetition-rate three-dimensional OH imaging using scanned planar laser-induced fluorescence system for multiphase combustion," Appl. Opt. **53**(3), 316–326 (2014).
15. V. A. Miller, V. A. Troutman, and R. K. Hanson, "Near-kHz 3D tracer-based LIF imaging of a co-flow jet using toluene," Meas. Sci. Technol. **25**(7), 075403 (2014).
16. R. Wellander, M. Richter, and M. Alden, "Time-resolved (kHz) 3D imaging of OH PLIF in a flame," Exp. Fluids **55**(6), 1–12 (2014).
17. T. C. Island, B. J. Patrie, M. G. Mungal, and R. K. Hanson, "Instantaneous three-dimensional flow visualization of a supersonic mixing layer," Exp. Fluids **20**(4), 249–256 (1996).
18. M. Zhang, J. Wang, W. Jin, Z. Huang, H. Kobayashi, and L. Ma, "Estimation of 3D flame surface density and global fuel consumption rate from 2D PLIF images of turbulent premixed flame," Combust. Flame **162**(5), 2087–2097 (2015).
19. W. Ng and Y. Zhang, "Stereoscopic imaging and reconstruction of the 3D geometry of flame surfaces," Exp. Fluids **34**(4), 484–493 (2003).
20. K. Y. Cheung and Y. Zhang, "Stereo imaging and analysis of combustion process in a gas turbine combustor," Meas. Sci. Technol. **17**(12), 3221–3228 (2006).
21. P. M. Danehy, B. F. Bathel, J. A. Inman, D. W. Alderfer, and S. B. Jones, "Stereoscopic Imaging in Hypersonic Boundary Layers using Planar Laser-Induced Fluorescence," in *26th AIAA Aerodynamic Measurement Technology and Ground Testing Conference* (AIAA, 2008), pp. 1–15.
22. X. Li and L. Ma, "Capabilities and limitations of 3D flame measurements based on computed tomography of chemiluminescence," Combust. Flame **162**(3), 642–651 (2015).
23. Y. Wu, Q. Lei, and L. Ma, "Experimental demonstration of 4D imaging in two-phase flows based on computed tomography at 5 kHz," Appl. Opt. **53**(24), 5547–5553 (2014).
24. X. Li and L. Ma, "Volumetric imaging of turbulent reactive flows at kHz based on computed tomography," Opt. Express **22**(4), 4768–4778 (2014).
25. W. Cai, X. Li, F. Li, and L. Ma, "Numerical and experimental validation of a three-dimensional combustion diagnostic based on tomographic chemiluminescence," Opt. Express **21**(6), 7050–7064 (2013).
26. J. Floyd, P. Geipel, and A. M. Kempf, "Computed Tomography of Chemiluminescence (CTC): Instantaneous 3D measurements and Phantom studies of a turbulent opposed jet flame," Combust. Flame **158**(2), 376–391 (2011).
27. J. Floyd and A. M. Kempf, "Computed Tomography of Chemiluminescence (CTC): High resolution and instantaneous 3-D measurements of a Matrix burner," Proc. Combust. Inst. **33**(1), 751–758 (2011).
28. M. Kang, Y. Wu, and L. Ma, "Fiber-based endoscopes for 3D combustion measurements: view registration and spatial resolution," Combust. Flame **161**(12), 3063–3072 (2014).
29. M. Kang, X. Li, and L. Ma, "Three-dimensional flame measurements using fiber-based endoscopes," Proc. Combust. Inst. **35**(3), 3821–3828 (2015).
30. W. Cai, X. Li, and L. Ma, "Practical aspects of implementing three-dimensional tomography inversion for volumetric flame imaging," Appl. Opt. **52**(33), 8106–8116 (2013).
31. W. Cai and L. Ma, "Hyperspectral tomography based on proper orthogonal decomposition as motivated by imaging diagnostics of unsteady reactive flows," Appl. Opt. **49**(4), 601–610 (2010).
32. W. Cai and L. Ma, "Applications of critical temperature in minimizing functions of continuous variables with simulated annealing algorithm," Comput. Phys. Commun. **181**(1), 11–16 (2010).
33. L. Ma, Q. Lei, Y. Wu, T. M. Ombrello, and C. D. Carter, "3D measurements of ignition processes at 20 kHz in a supersonic combustor," Appl. Phys. B **119**(2), 313–318 (2015).

1. Introduction

Optical diagnostics based on laser induced fluorescence (LIF) have been extensively researched and applied in the past [1, 2]. LIF-based diagnostics have been demonstrated as a powerful and versatile tool for flow visualization and measurements. Many key flow parameters, including species concentration [3, 4], temperature [5], and mixture fraction [6–8], can be inferred from LIF measurements. However, past work has been largely limited to measurement at a point, along a line, or across a two-dimensional (2D) plane [9–11], while turbulent flows are inherently 3D in space. Therefore, there is a strong motivation to extend the LIF technique for volumetric measurements.

One possible approach of such extension is a scanning PLIF (planar laser induced fluorescence) technique, in which the excitation laser sheet used in the PLIF technique was scanned across multiple spatial locations sequentially, and then the 2D measurements obtained at these locations were stacked together to form a 3D measurement [12–16]. Even though this approach was conceptually straightforward and has been explored earlier [12, 17], it is not trivial to obtain quantitative measurements with sufficient temporal and spatial resolution. Even with the latest advancement in high repetition rate lasers, high frame rate

cameras, and the corresponding optics and electronics, measurements following the scanning approach have been limited to a temporal resolution of 1 kHz and a spatial resolution on the order of 1 mm in the direction of the scanning [14–16]. Higher spatiotemporal resolutions are desired or required for many flows of practical interest [18]. Another possible approach involved a combination of stereoscopic imaging [19, 20] and PLIF. This approach uses a relatively thick laser sheet (instead of a thin sheet as in regular PLIF) to illuminate the target flow and capture the LIF images from two different view angles. Spatial information in the depth direction can then be inferred via stereoscopic algorithms [4, 21]. Since no scanning is required in this approach, the temporal resolution of this approach is only limited by the speed of the laser and the camera, and measurements at 500 kHz have been reported [4]. However, the drawback is that it is difficult to extract spatial information in the depth direction and the spatial resolution in the width and height directions is degraded due to the use of a thick illumination sheet [21].

Based on the above understanding of approaches explored in the past, this work reports a new approach, which is termed VLIF (volumetric LIF), to extend LIF for 3D measurements. The VLIF approach combined LIF with computed tomography to obtain 3D measurements volumetrically without scanning, thusly offering the potential to obtain 3D measurements instantaneously and improve the spatial resolution in the scanning direction. More specifically, the VLIF approach uses a thick laser slab (in contrast to the thin laser sheet used in PLIF) to excite the target species volumetrically. The LIF signals emitted by the target species are then captured by multiple cameras from different orientations simultaneously. Because the LIF signals are generated volumetrically, the images captured by the cameras are line-of-sight integrated (which are termed *projections*). A tomographic algorithm [22–27] is then employed to reconstruct the 3D distribution of the target species based on such projection measurements, as elaborated in Sections 2 immediately below.

2. Experimental arrangement

The experimental setup was schematically illustrated from the top view as shown in Fig. 1(a). As shown in the center of Fig. 1(a), the target flow was a turbulent jet flow consisting of nitrogen and iodine vapor (I_2). The exit diameter of the jet was 6.35 mm. The I_2 vapor was generated by heating iodine crystals (contained in a vessel) in a water bath to a temperature of 200 °F (93 °C). A carrying dry nitrogen flow was passed through the vessel to introduce the I_2 vapor into the target flow. The mole fraction of the I_2 vapor in the target flow was therefore controlled by the vapor pressure of I_2 under the bath temperature and the flow rate of the nitrogen gas, and the maximum mole concentration of the I_2 vapor in the target flow was estimated to be 4% in the experiments performed here. The design of the seeding concentration for the VLIF measurements was similar to that for traditional PLIF measurements, involving a trade-off among several factors such as signal level, disturbance to the chemical composition of the target flow, and practicality of seeding the desired concentration. The VLIF technique was then applied to measure the relative concentration of the seeded I_2 in 3D. Note that other flow properties can be calculated as well, such as 3D mixtures fraction if the tracer can serve as a conserved scalar in the target flow (similar to the calculation of 2D mixture fraction based on PLIF). The use of I_2 tracer for mixture fraction measurement has been discussed in [8].

In some of the experiments, a rod (with a diameter of 3.18 mm) was placed at the exit of the jet, to increase the complexity of the flow structures (and also to create an easily recognizable pattern of the flow to facilitate validation). Based on the flow configuration, the following Cartesian coordinate system was defined as shown in the figure: the center point of the jet at the exit plane was defined as the origin, the flow direction was defined as the z axis, and the y axis was defined along the direction of the rod.
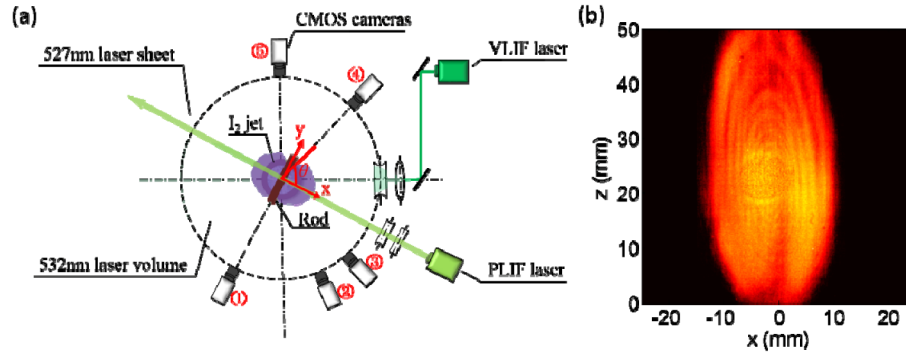
Fig. 1. Panel (a): experimental setup from the top view. Panel (b): the spatial profile of VLIF laser intensity at $y = 0$.

The VLIF technique used the output of a pulsed Nd: YAG laser (Quanta-Ray Spectra-Physics), labeled as VLIF laser in Fig. 1(a) at 532 nm to excite the seeded I_2 vapor. The pulse duration was about 8 ns, the repetition rate was 10 Hz, and the pulse energy was 600 mJ. The excitation laser pulses were expanded by a series of lenses into a thick laser slab so that it can illuminate a volume of 50 mm × 50 mm × 50 mm, and the entire target flow was excited volumetrically.

The VLIF signals generated by the volumetric excitation were then captured by five CMOS cameras (four Photron SA4s and one SA5) as shown in Fig. 1(a). All cameras were aligned in the x-y plane and therefore their orientations were completely specified by θ, defined as the angle formed by the optical axis of a camera relative to the positive x direction as shown. The focal length and f-number of the lenses used on all cameras were 105 mm and 2.8, respectively. Each lens was equipped with a 532 ± 10 nm OD4 notch filter to block any scatter of the excitation laser. The operation of the laser and cameras was synchronized using control electronics. Prior to any measurement, a calibration target was used to determine the orientation and location of the cameras using a view registration program [28, 29]. The orientations of camera 1 through 5 were determined to be θ = 270.0°, 311.8°, 341.9°, 73.7° and 111.1°, respectively, with an accuracy estimated to be within 0.5°. All the cameras were approximately 420 mm away from the target.

A simultaneous PLIF measurement was also performed by exciting the LIF transition of I_2 with another laser (labeled as the PLIF laser), with the purpose of providing a direct validation for the VLIF measurements. More specifically, the PLIF measurements provided a 2D image at a certain cross section of the 3D flow, which can be compared against the 3D reconstruction at the same cross section. The PLIF laser (Photonics Industries DM20 - 527 DH) generated laser pulses at a wavelength of 527 nm, with a duration of 440 ns, a pulse energy of 12 mJ, and a repetition rate of 5 kHz. The PLIF laser pulses were focused into sheets with a thickness less than 0.8 mm. The PLIF laser was aligned along the x axis (i.e., perpendicular to rod). To best utilize the cameras available to this project, the VLIF laser, PLIF laser, and camera 1 (which was aligned perpendicular to the PLIF laser sheet) were configured in such a way that camera 1 captured the VLIF and PLIF signal sequentially in two consecutive frames, and the temporal separation between these two frames was 0.2 ms. As a result, even though both the VLIF and PLIF techniques were able to generate single-shot measurements and therefore can be applied to highly turbulent flows, experiments in this work were performed under moderate turbulence levels (with a Reynolds number of 2000 defined based on the jet exit diameter), such that the flow can be approximately considered frozen during the 0.2 ms separation to make the PLIF and VLIF measurements comparable.

Before performing measurements in turbulent flows, the first step was to characterize the profile of the VLIF and PLIF laser pulses, since the LIF signal depended on both target concentration field and laser intensity distribution. To accomplish this goal, a dye cell, with a

length and height both of 50 mm and a thickness of 0.5 mm, was fabricated. This cell therefore can hold a thin layer of uniform dye solution (with a thickness of 0.5 mm). The solvent was ethanol and the dye was Rhodamine 6G, which can be excited by both the 532 nm and 527 nm laser pulses. The dye cell was then placed at different locations in the measurement volume. At each location, the dye cell was aligned perpendicular to the propagation direction of the laser pulses to be illuminated by both the PLIF and VLIF lasers. Due to the thinness of the dye solution in the cell, the integration effects in the dye were neglected and the measurement at each location was taken as the intensity distribution of the corresponding laser at that spatial location. Figure 1(b) shows an example of the 2D intensity profile of the VLIF laser measured at $y = 0$. The intensity profile was apparently non-uniform, necessitating such characterization *a priori*. Compiling the measurements obtained at a series of locations then provided the spatial distribution of both the VLIF and PLIF lasers.

3. Tomographic reconstruction

After the characterization of the laser profiles, experiments were then performed in another dye cell (a cubical cell with a side length of 50 mm) to validate the VLIF tomographic algorithm under controlled conditions. The tomographic algorithm was based on a variation of the Algebraic Reconstruction Technique (ART), which has been validated and demonstrated extensively in the previous work for both absorption- and emission-based tomographic problems [25–27, 30, 31]. The tomography algorithm analyzes how many photons are collected on a given pixel and where these photons are emitted from the measurement volume. The tomography algorithm did not rely on assumptions of parallel beam or in-focus imaging (which have limited validity in practice especially for any extended measurement volume). As a result, it is not required for the entire measurement volume (with a dimension of 50 mm) to be within the depth of field of the cameras (which was about ~1 mm for all the cameras). However, LIF-based tomography introduces a fundamental difference when the absorption is not negligible, because the intensity of the excitation laser pulse varies as it propagates through the measurement volume due to absorption, and the variation depends on the concentration of the sought distribution of the target species.

In this work, the VLIF problem was solved by iterating an ART algorithm on the target concentration field layer by layer iteratively. More specifically, the algorithm consisted of four steps. In the first step, the computation domain was divided into multiple layers (and the first layer was defined as the layer the VLIF laser first interacted with). In the second step, the 3D reconstruction of the concentration of the target species was performed in the first layer. The laser intensity in the first layer was only attenuated by the target species in the first layer and this attenuation can be neglected if the layer was sufficiently thin. Therefore the laser intensity in the first layer was known (i.e., identical to the incident one that characterized *a priori* as shown in Fig. 2(a)). Therefore, with the laser intensity known, the 3D reconstruction in the first layer can then be solved by the ART algorithm. In the third step, with the 3D concentration of the target species obtained from the second step, the intensity profile of the laser exiting the first laser (i.e., entering the second layer) can then be calculated, which was taken as the laser profile in the second layer (again assuming sufficiently thin layers). Hence, the 3D reconstruction in the second layer can be performed. In the fourth step, the operations described in steps two and three were iterated on the remaining layers until convergence was achieved. Detailed description of the algorithm and its numerical validation will be elaborated elsewhere. Here we focus on the experimental validation of the algorithm and its application.

Figure 2 shows a set of example validation results obtained in the 50 mm × 50 mm × 50 mm cubical dye cell using the algorithm described above. This cell was filled with the same Rhodamine 6G solution and placed in the measurement volume. The dye solution was excited with the 532 nm VLIF laser volumetrically. The LIF emissions were measured by all five cameras, based on which a tomographic reconstruction was performed using the algorithm described above to obtain the 3D distribution of the dye concentration (which should be

simply a uniform distribution because the dye solution was well mixed). The computational domain was taken to be 50 mm × 50 mm × 50 mm, identical to the cubical dye cell. The domain was then discretized into 120 × 120 × 120 voxels, resulting in a 3D spatial resolution of 0.42 mm × 0.42 mm × 0.42 mm in the reconstruction. The discretization was designed by a consideration of both practical and fundamental factors. Practically, the computational cost and memory requirement scale proportionally to the discretization. Fundamentally, when the number of unknowns (i.e. number of voxels) in the tomography problem exceeds the number of independent equations provided by the measured projections (i.e. number of pixels in the measured projections), the problem becomes under-determined. With the cameras and imaging optics available in this work, the number of pixels providing useful information was approximately 1.8×10^6, and a discretization of 120 × 120 × 120 resulted in a total of ~1.7×10^6 voxels.
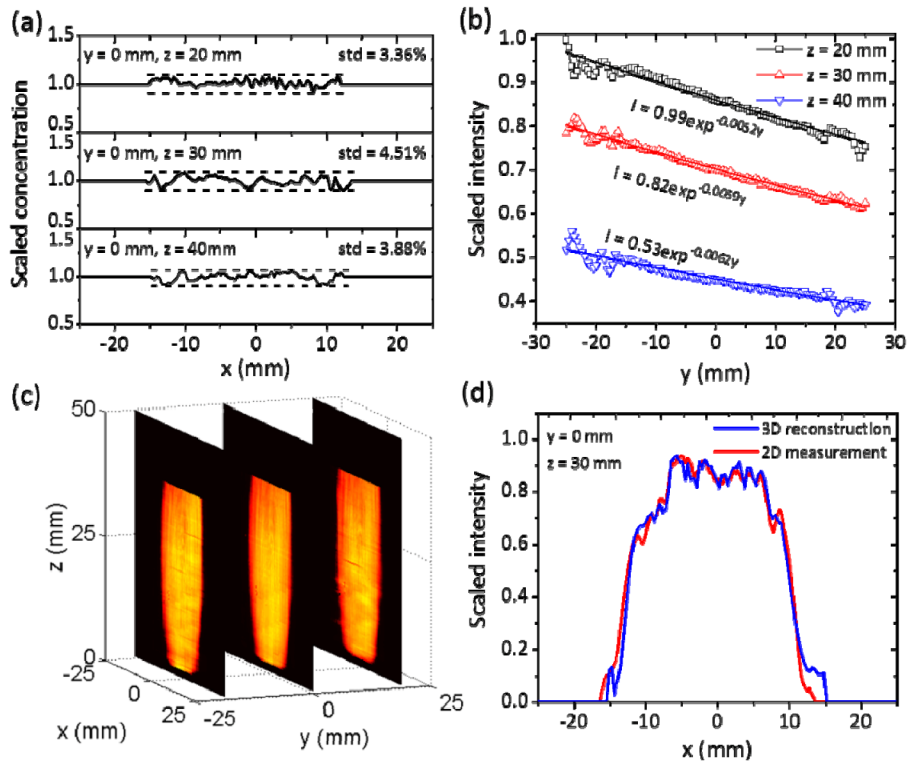

Fig. 2. Controlled VLIF experiments performed in a dye cell. Panel (a): dye concentration at three locations obtained from 3D VLIF measurements. Panel (b): scaled laser intensity along the VLIF laser path at three different z locations (z = 20, 30 and 40 mm). Panel (c): laser intensity at three locations obtained using the 3D VLIF reconstruction algorithm. Panel (d): comparison of the laser intensity obtained by 3D reconstruction and direct 2D measurement.

Figure 2(a) shows the reconstructed concentration (normalized) at several z locations (z = 20, 30 and 40 mm) along the central plane of the dye cell (i.e., y = 0 mm). As seen from Fig. 2(a), the reconstructed concentration agreed with the expected uniform distribution closely, with a std (standard deviation) less than ~5%. Reasons for such deviation and future improvement will be examined more closely at the end of this section. To confirm that appreciable attenuation occurred in these measurements, Fig. 2(b) shows the laser intensity measured along the laser propagating direction (i.e., along the y axis) at three different z locations (i.e. z = 20, 30 and 40 mm). These measurements were made by focusing the VLIF laser into a thin sheet, propagating the sheet through the dye cell, and measuring the LIF

emissions at different y locations. As seen from Fig. 2(b), the intensity (I) of the excitation laser was attenuated appreciably due to absorption, and a fit of the data confirmed that the absorption follows the exponential Beer-Lambert relationship. The reconstruction algorithm was insensitive to the magnitude of absorption under the conditions in this work, primarily for two reasons. First, the absorption was not very strong (~20% in the dye cell test shown here and less than 5% in the flow measurements) and the media remained optically thin. Second, the algorithm was designed to perform reconstruction under appreciable absorption. Though it is an interesting topic for future research to examine the accuracy and applicability of the algorithm under strong absorption (i.e., in an optically thick media).

Results in Fig. 2(c)-2(d) provide another validation of the VLIF reconstruction algorithm in an absorbing media by exploiting the duality of the tomography algorithm. More specifically, the problem of reconstructing the concentration field with known laser intensity field (as solved in Fig. 2(a)) is equivalent to reconstructing the laser intensity field with known concentration field, and both problems were solved by the algorithm described in Section 3. Based on such duality, the VLIF algorithm was applied to reconstruct the 3D laser intensity field based on the projections measured from the dye cell under the same discretization scheme used in Fig. 2(a). Again, in this reconstruction, the dye solution was taken as an input known *a priori* (i.e., a uniform distribution). Figure 2(c) shows the laser intensity at three different locations (the 20th, 60th and 100th layer in the y direction) obtained from this reconstruction. To examine the reconstruction quantitatively, Fig. 2(d) compares reconstructed laser intensity against that directly measured (i.e., the one shown in Fig. 1(b)) along a line ($y = 0$ and $z = 30$ mm). As seen in Fig. 2(d), the 3D reconstruction and the measurement agree well both at an overall and detailed level. The variation was also within ~5%, similar to that observed in Fig. 2(a). The experiments performed here and the reconstruction algorithm also provide an approach to characterize the 3D distribution of the laser intensity.

In summary, controlled measurements were performed in a dye cell to provide experimental validation to the VLIF reconstruction algorithm. Exploiting the duality of the problem, the algorithm was validated both via comparison between reconstructed dye concentration field against the known concentration field, and also via comparison between reconstructed laser intensity field against the measured intensity field. Both validations showed an agreement within ~5%. Two major factors causing such disagreement included the reconstruction algorithm and measurement error caused by pulse-to-pulse variation of the laser intensity. First, according to our numerical simulations using phantoms, the reconstruction algorithm was able to solve the VLIF problem within 1~2% accuracy with error-free projections (here accuracy was defined following [24] as the overall difference between the reconstructed distribution and the phantom relative to the overall magnitude of the phantom). The current algorithm was based on the iteration of the ART, and alternative algorithms (e.g., based on simulated annealing [31, 32]) are being explored to improve the reconstruction accuracy. Second, the shot-to-shot variation of the laser pulses was measured to be ~1.1% both in terms of the pulse energy and spatial distribution (defined as the std over 50 shots), while the laser profile characterization was not performed *in situ* (e.g., the 3D and 2D measurements compared in Fig. 2(d) were taken at different times). Possible approaches to reduce uncertainty caused by this factor include the use of a more stable laser, monitoring the laser intensity *in situ* with additional cameras, or performing the measurement in the saturated regime.

4. Results from turbulent flows

With the experimental setup and tomographic algorithms developed in the previous sections, this section reports single-shot VLIF measurements of 3D distribution of I_2 vapor in turbulent jet flows.

Figure 3 shows a set of example projections captured by camera 1 through 5, displaying an incompletely developed jet flow with two branches generated by the rod placed at the exit of the jet. Figure 3(a) shows the PLIF image obtained by camera 1, and Fig. 3(b)-3(f) show the simultaneously measured VLIF projections by camera 1 through 5, respectively. As mentioned earlier, the VLIF projections were measured 0.2 ms after the PLIF image, and this delay was negligible for this flow (with a Reynolds number of 2000 defined based on the jet exit diameter) so that the PLIF and VLIF measurements were considered to be simultaneous. All projections had a resolution of 600 × 600 pixels, and each pixel corresponded to a physical dimension of 0.06 × 0.06 mm. Both the PLIF image and VLIF projections were single-shot measurements. Note that the PLIF image in Fig. 3(a) appeared clearer and sharper than the VLIF projection because the VLIF projections **(Fig. 3(b)-3(f))** were line-of-sight integrated.
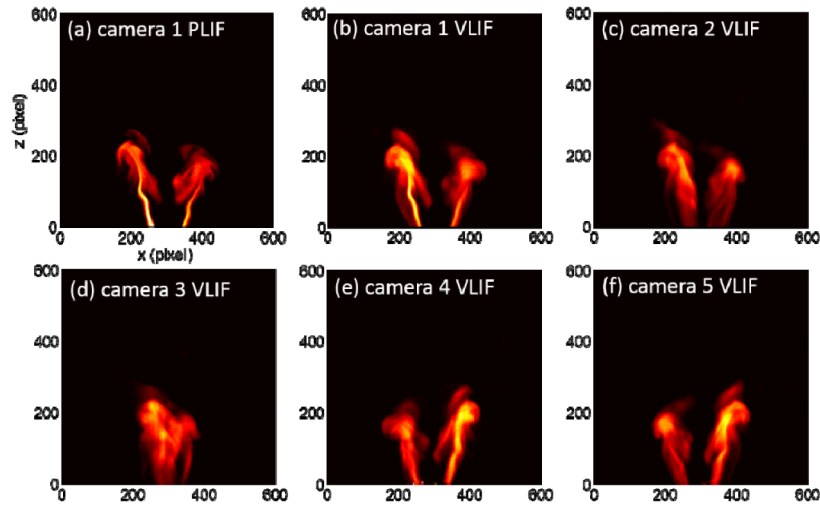

Fig. 3. A set of example projections measured by camera 1 through 5. Panel (a): the PLIF image captured by camera 1. Panels (b) - (f): the VLIF projections captured by camera 1 through 5.

Based on the projections, the 3D distribution of the I_2 vapor concentration in the jet flow was reconstructed using the tomographic algorithm described above. Figure 4 shows an example reconstruction obtained using the projections shown in Fig. 3. This reconstruction was performed in a computational domain of 35.5 mm × 35.5 mm × 35.5 mm, sufficient to encompass the entire target flow as seen in Fig. 3. This computational domain was discretized into 120 × 120 × 120 voxels (~1.7×10^6), resulting in a nominal spatial resolution of 0.30 mm. Figure 4(a) shows a 3D rendering of the relative I_2 concentration, illustrating the overall V-shape of the flow. The iso-surface value in Fig. 4(a) was set to a numerical value of 11% of the maximum intensity of the reconstructed I_2 concentration in the domain of interest, a value chosen to provide differentiation against background noise and to preserve the contour of the I_2 concentration field. To better present the 3D reconstruction, Fig. 4(b) shows three planar slices of the reconstruction at three different y locations (corresponding to the 50th, 60th, 70th layer in the y direction). Figure 4(b) shows that the 3D reconstruction also captured the flow feature at a more detailed level. For example, the 60th layer corresponded to the central plane of the jet flow (i.e. $y = 0$), and therefore the overall I_2 concentration on this layer should be higher than the other two layers due to less entrainment (more ambient air was entrained into the jet in its outer portions than the central portions, resulting in more dilution and relatively lower I_2 vapor concentration in the outer portions). This feature was clearly captured by the 3D reconstruction shown in Fig. 4(b). Accompanying the results in Fig. 4 is a media file

(Visualization 1) that shows an animated 360° rotation view based on the 3D data used in Fig. 4. The rendering in Fig. 4 was based on an iso-surface at one chosen value of the 3D reconstruction, while the animation was based on multiple iso-surfaces, each plotted with a different opacity, to better illustrate the 3D structure of the flow.
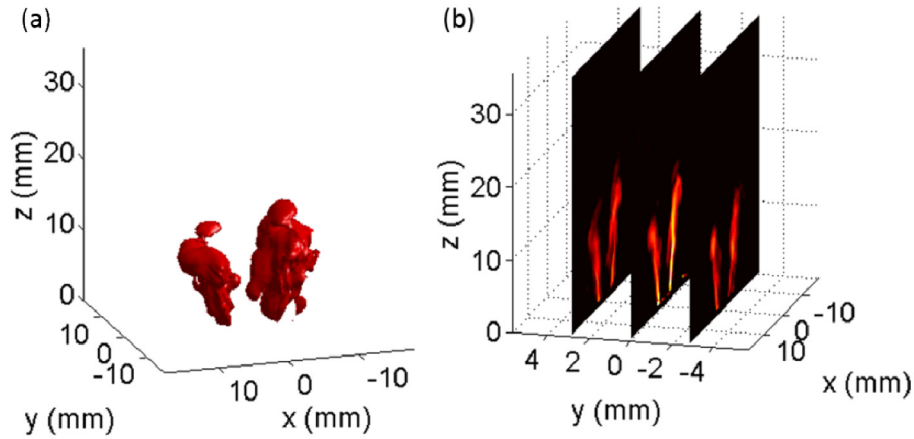

Fig. 4. Panel (a) 3D VLIF measurement of a jet flow (see also Visualization 1), Panel (b) three 2D slices of the measurement (panel b).
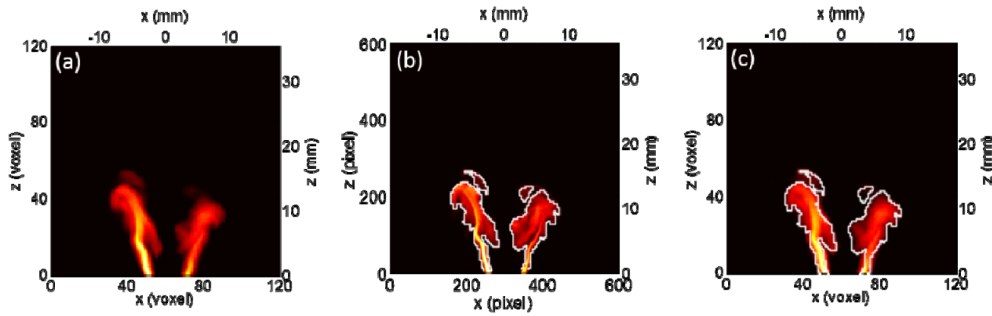

Fig. 5. Comparison of VLIF against PLIF in an under-developed turbulent jet flow. Panel (a): the VLIF reconstruction at the central layer at y = 0. Panel (b): PLIF measurement of the flow at its central plane (captured by camera 1). White line shows the edge extracted from the image. Panel (c): panel (a) overlapped with the edge extracted from the PLIF image (i.e., the white line shown in panel (b)).

To further validate the above 3D VLIF reconstructions, Fig. 5 directly compares the VLIF against the PLIF measurements. Figure 5(a) shows the VLIF reconstruction at the central layer at y = 0, (i.e. layer 60th as shown in in Fig. 4(b)). Figure 5(b) shows the PLIF image measured by camera 1 also at the central layer (i.e., the same image shown in Fig. 3(a)). A comparison between Figs. 5(a) and 5(b) suggests agreement at both overall and detailed level. For example, both the VLIF and PLIF measurements revealed the left branch to be taller and have an overall higher I_2 concentration than the right branch. The comparison between Figs. 5(a) and 5(b) also shows the differences in spatial resolution between the VLIF and PLIF measurements. The VLIF measurement contained more imaging elements than the PLIF measurements (a total of ~1.7×10^6 voxels in the VLIF versus 0.36×10^6 pixels in the PLIF). However, due to the volumetric nature of the VLIF measurement, the PLIF measurement had a superior pixel resolution in a plane as shown in Figs. 5(a) and 5(b). As aforementioned, the nominal spatial resolution of the VLIF measurement was 0.42 mm, calculated by dividing the dimension of the measurement volume with the discretization (i.e., 50 mm/120 = 0.42 mm). This nominal resolution represents the highest possible resolution that can be obtained. The

actual resolution will be worse than the nominal resolution due to the factors such as measurement and reconstruction uncertainty. The comparison between VLIF and PLIF shown in Fig. 5(c) provides a way to estimate the actual resolution. The spatial resolution of the PLIF measurements was estimated to be 0.059 mm in this work, sufficiently higher than of the nominal VLIF resolution. We examined which level of details captured by the PLIF can be resolved by the VLIF using the comparisons such as shown in Fig. 5(c). Based on this examination, the actual spatial resolution of the VLIF was estimated to be 0.71 mm, which was worse than (but on the same order as) the nominal resolution of 0.42 mm.
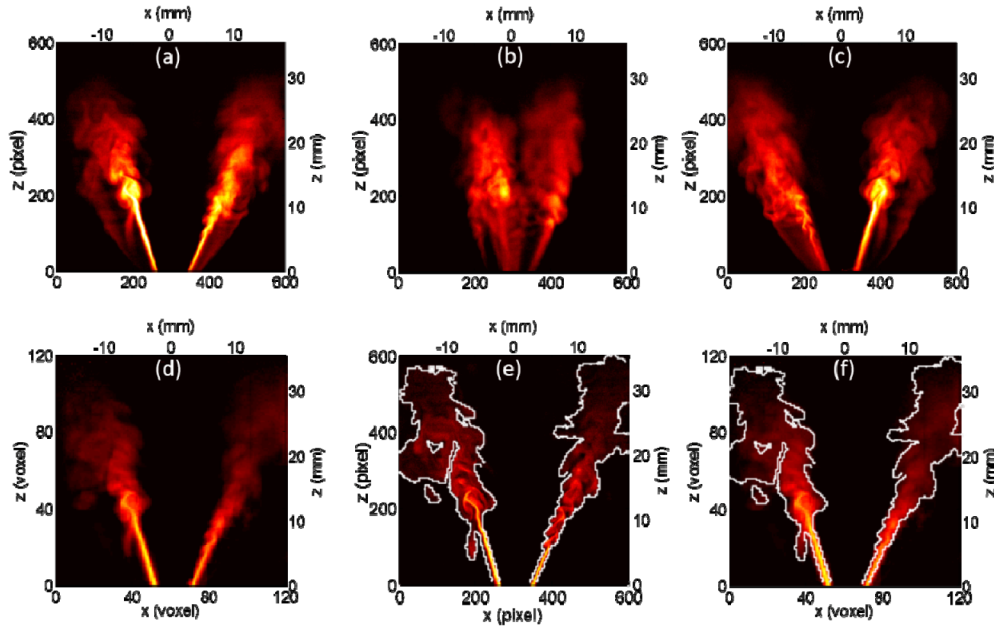

Fig. 6. Comparison of 2D reconstructed slice against the experimental PLIF and VLIF projection in a fully developed turbulent flow (see also Visualization 2). Panel (a)-(c): three of the five projections used in the VLIF reconstruction, captured by camera 1, 3, and 4, respectively. Panel (d): the VLIF reconstruction at the central layer at y = 0. Panel (e): PLIF measurement of the flow at its central plane (captured by camera 1). White line shows the edge extracted from the image. Panel (f): panel (d) overlapped with the edge extracted from the PLIF image (i.e., the white line shown in panel (e)).

Therefore, with the current status of the VLIF technique demonstrated in this work, it can overcome the planar nature of PLIF and resolve the three dimensionality of turbulent flows, but still cannot compete with PLIF in terms of pixel resolution in a plane. Further research is undergoing in our group to improve the spatial resolution of the VLIF technique while maintaining its single-shot and instantaneous nature. To facilitate a more quantitative comparison, also shown in panel Fig. 5(b) is the edge of the flow structure extracted from the PLIF image (the white lines) with a thresholding algorithm [33]. Figure 5(c) then overlaps the edge on top of the VLIF slice shown in Fig. 5(a). Good agreement can be observed in Fig. 5(a). For instance, the two detached flow regions in each branch were measured by both the VLIF and PLIF techniques.

Lastly, Fig. 6 shows another example of the comparison between the VLIF and PLIF techniques in a fully developed turbulent flow. Figure 6(a)-6(c) show three of the five projections used in the VLIF reconstruction, captured by camera 1, 3, and 4, respectively. Figure 6(d)-6(f) are parallel to Fig. 5(a)-5(c), showing the central slice taken from the 3D VLIF measurement, the corresponding PLIF measurement and its edge extracted, and the overlap of the edge with the VLIF slice, respectively. An accompanying media file

(Visualization 2) was again created to better illustrate the 3D structure of this flow using the same method as in Visualization 1. These results further illustrate the good agreement between VLIF and PLIF measurements.

5. Summary

This work reports the experimental demonstration of single-shot measurements in turbulent flows vapor using volumetric laser induced fluorescence (VLIF). Single-shot 3D measurements (with a measurement duration of a few ns) were demonstrated in a 50 mm × 50 mm × 50 mm volume with a total of 120 × 120 × 120 voxels (resulting in a nominal spatial resolution of 0.42 mm in all three dimensions). The measurements were performed based on the LIF signal of iodine (I_2) vapor seeded in the flow. The VLIF technique excited the seeded I_2 vapor volumetrically by a thick laser slab. The volumetric LIF signals emitted were then simultaneously collected by a total of five cameras from five different orientations, based on which a 3D tomographic reconstruction was performed to obtain 3D measurements. To validate the reconstruction algorithm and VLIF measurements, static cell measurements and simultaneous PLIF measurements were also performed. The static cell experiments provided controlled tests to the reconstruction algorithm by the use of a dye cell with a known (i.e., uniform) concentration field. The PLIF measurement performed simultaneously with the VLIF provided a direct comparison for validation. Such comparison, besides providing a validation of the VLIF measurements, suggests that the actual spatial resolution of the VLIF technique to be ~0.71 mm, compared to the nominal resolution of 0.42 mm. The comparison also shows that at the status of the VLIF demonstrated in this work, the PLIF technique still offers superior spatial resolution in a plane even though the VLIF technique enables more total imaging elements volumetrically and resolves the three dimensionalities of turbulent flows.

Acknowledgment